NANO-MICRO LETTERS ARTICLE
www.nmletters.org

RhB Adsorption Performance of Magnetic Adsorbent Fe_3O_4/RGO Composite and Its Regeneration through A Fenton-like Reaction

Yalin Qin, Mingce Long*, Beihui Tan, Baoxue Zhou

(Received 15 October 2013; accepted 21 December 2013; published online 20 March 2014)

Abstract: Adsorption is one of the most effective technologies in the treatment of colored matter containing wastewater. Graphene related composites display potential to be an effective adsorbent. However, the adsorption mechanism and their regeneration approach are still demanding more efforts. An effective magnetically separable absorbent, Fe_3O_4 and reduced graphene oxide (RGO) composite has been prepared by an in situ coprecipitation and reduction method. According to the characterizations of TEM, XRD, XPS, Raman spectra and BET analyses, Fe_3O_4 nanoparticles in sizes of 10-20 nm are well dispersed over the RGO nanosheets, resulting in a highest specific area of 296.2 m^2/g. The rhodamine B adsorption mechanism on the composites was investigated by the adsorption kinetics and isotherms. The isotherms are fitting better by Langmuir model, and the adsorption kinetic rates depend much on the chemical components of RGO. Compared to active carbon, the composite shows 3.7 times higher adsorption capacity and thirty times faster adsorption rates. Furthermore, with Fe_3O_4 nanoparticles as the in situ catalysts, the adsorption performance of composites can be restored by carrying out a Fenton-like reaction, which could be a promising regeneration way for the adsorbents in the organic pollutant removal of wastewater.

Keywords: Magnetic adsorbent; Fe_3O_4 nanoparticles; Reduced grapheme oxide; Fenton-likereaction; Regeneration

Citation: Yalin Qin, Mingce Long, Beihui Tan and Baoxue Zhou, "RhB Adsorption Performance of Magnetic Adsorbent Fe_3O_4/RGO Composite and Its Regeneration through A Fenton-like Reaction", Nano-Micro Lett. 6(2), 125-135 (2014). http://dx.doi.org/10.5101/nml.v6i2.p125-135

Abbreviation

Q_e — Equilibrium adsorption capacity of adsorbent, mg/g;
C_i — The initial aqueous phase concentration of absorbates, mg/L;
C_e — The equilibrium concentration of absorbates, mg/L;
V — The volume of solution, mL;
M_s — The mass of adsorbent, g;
Q_{max} — The maximum adsorption capacity of adsorbent, mg/g;
K_L — The Langmuir constant, L/mg;
K_f — Freundlich constant, L/g;
n — Freundlich constant.

Introduction

Colored matter containing wastewater discharged from dyeing, textile, leather, cosmetics or food industries has brought serious environmental problems in our daily life. Even at a low concentration, dyes in water would bring aesthetically displeasing, and most of them are toxic to both aquatic life and humans [1]. The complex conjugated molecular structures make them stable and recalcitrant to oxidant and bacteria, also resistant

School of Environmental Science and Engineering, Shanghai Jiao Tong University, Shanghai 200240, China
*Corresponding author. E-mail: long_mc@sjtu.edu.cn

to be bleached by sunlight. Accordingly, traditional biological or chemical oxidation methods are difficult to remove them from wastewater. Simultaneously, dyes are always highly soluble in water, rendering them hard to be dealt with by precipitation or flocculation. Therefore, cost-effective method is still urgently demanded to remove colored substance from wastewater. Adsorption is an effective and classic depth processing in the field of wastewater treatment, by which a substance at the interfacial layer of the adsorbent would accumulate owing to the operation of surface forces [2]. Compared to other advanced water-treatment technology, adsorption has such merits as a low invest-cost, simplicity of design and operation, and no discharge of harmful substances. Although the history of adsorption in wastewater treatment is more than one hundred years, there are still two challenges in the practical applications. One is to realize selective adsorption, which is the prerequisite for recovering valuable substances from wastewater without being disturbed by coexisting matters [3,4]. Another is to obtain adsorbents possessing excellent adsorption performance and the ability to be facilely separated and regenerated, which is significant to lower the operating cost [5,6].

In previous years, carbonaceous materials, including active carbon and carbon nanotubes, have been widely investigated and applied in the removal of diverse pollutants from water due to their high adsorption capacity [1,7]. Compared with them, graphene and graphene oxide (GO) nanosheets, a type of two-dimensional nanomaterial with a single layer framework of six-member carbon rings, also show strong adsorption ability for both organic or inorganic pollutants because of their large theoretical specific surface area of 2630 m^2/g and special π-π conjugate planar geometric structure [8-12]. Moreover, the oxygen-containing groups and surface amphiphilicity can be tuned by synthesizing modified GO or reduced GO (RGO) for specific adsorption objectives [13,14]. On the other hand, multifunctional graphene-related nanocomposites would bring additional properties to graphene and become a focused field of graphene materials [11,15,16]. Among them, incorporation of magnetic nanoparticles with graphene has attracted tremendous attention. The inherent superparamagnetic behavior of magnetic nanoparticles enables them to be easily separated and collected by an external weak magnetic field [17,18]. Moreover, the presence of Fe_3O_4 nanoparticles can prevent the aggregation and restacking of graphene sheets, and consequently retain a high surface area [19]. In addition, Fe_3O_4 nanoparticles can serve as both a powerful adsorbent [17,20] and a catalyst for heterogeneous Fenton-like reaction [21,22]. The superparamagnetic Fe_3O_4 nanoparticles possess excellent adsorption capacity for arsenic removal [17], and the performance was much improved when they are dispersed over RGO to form a hybrid adsorbent [23]. In addition, considering the accumulated organic molecules at the interface layer by adsorption is similar to a concentrated process, combining Fenton-like oxidation after adsorption would significantly enhance the reaction kinetics and possibly develop into a new regeneration approach [5].

In general, the Fe_3O_4/GO (or RGO) nanocomposites can be synthesized by solvothermal, self-assembly with covalent bond, and in-situ chemical coprecipitation methods, and display efficient adsorption performance in the removals of organic dyes and inorganic metal ions in wastewater [19,23-27]. The abundant oxygen-containing groups on GO enable a hydrogen bond and electrostatic interactions with organic adsorbates, while the hydrophobic polyaromatic islands of unoxidized benzene rings of RGO offer hydrophobic interaction and π-π stacks toward the organic molecules, especially conjugation molecules. However, much more efforts are required to understand the optimized structural factors for adsorption. Furthermore, it was found that under a photo-Fenton reaction GO would transform into graphene quantum dots [28]. Although GO is unstable in the Fenton conditions, RGO is recalcitrant in the heterogeneous Fenton-like reaction, because the less oxygen containing groups in RGO makes the initial decomposition unfeasible [28], and the oxidation species in the Fenton-like system are localized over the surface of catalysts and less accessible to the graphene partial. Due to the large specific surface area, tunable structures and components of RGO, its application in Fenton(-like) reactions has attracted increasing attentions in the latest years [29-31].

Herein, a Fe_3O_4/RGO composite with efficient adsorption performance for rhodamine B (RhB) removal has been synthesized by optimizing the iron source, and the structural controllable adsorption mechanism was discussed by the analyses of isotherms and kinetics. Moreover, the regeneration of the adsorbent has been preliminarily studied via a way of heterogeneous Fenton-like reaction.

Experimental

Materials

Ferrite chloride ($FeCl_3 \cdot 6H_2O$), graphite (Spec. pure) and active carbon (AC) powder were procured from Sinopharm Chemical Reagent Co., Ltd. RhB were obtained from Shanghai Hyperheal Biotech Co., Ltd. Ferrous chloride ($FeCl_2 \cdot 4H_2O$) was purchased from Aladdin Chemistry Co. Ltd. All chemicals used in this study without special states were of analytical grade and used as received. All solutions were prepared with deionized water.

Synthesis of Fe_3O_4/RGO adsorbents

Graphene oxide was prepared by a modified Hummers' method [32, 33]. Briefly, graphite oxide was obtained by oxidizing graphite powder with the presence of H_2SO_4, $NaNO_3$ and $KMnO_4$. The graphite oxide was washed with diluted HCl solution and exfoliated by ultrasonic treatment at 400 W for 30 min. The Fe_3O_4/RGO adsorbents were synthesized through an in situ method. In a typical synthesis, $FeCl_2{\cdot}4H_2O$ and $FeCl_3{\cdot}6H_2O$ (weight ratio 3.17) were firstly dissolved in 60 mL GO aqueous suspension (1 mg/mL). The mixture was mechanical agitated in a nitrogen atmosphere at 90°C for 20 min, to ensure that ferric and ferrous salts were completely dissolved and anchored at the surface of GO nanosheets by chemical interactions. Then 20 mL aqueous ammonia was dropwise added, following with 4 h reaction at 90°C to complete the precipitation and formation of Fe_3O_4 and the reduction of GO. Finally the precipitation was magnetically separated, washed with copious water, and vacuum dried overnight at 60°C. The obtained dark powder is a composite of Fe_3O_4 and RGO. By changing the amount of iron source, various composites with different theoretic weight ratios of Fe_3O_4 (according to the amount of total iron dosages) to RGO (according to the GO dosages) were synthesized, that is 1:1, 2:1, 3:1 and 4:1 and assigned as M-1 to M-4, respectively. The control sample of Fe_3O_4 nanoparticles were also prepared according to the same procedure but without the addition of GO in the reaction solution.

Adsorption kinetics and isotherms

The kinetics of the adsorption process was determined in batch experiments with 50 mg/L RhB solutions. A 100 mL volume of the test solution and 0.2 g weight of adsorbent were shaken in a flask at a speed of 150 r/min at 30°C in a thermostatic oscillatory water bath. At several points in time, 5 mL sample was taken out from the water bath, and the supernatant solution was collected by preliminarily magnetic separation and subsequently centrifugation to ensure completely removal of solid adsorbents. The residual concentration was analyzed by a UNICO UV-1202 spectrometer. The control (no sorbent) test displays there is negligible change of the dye concentration in the whole process.

RhB adsorption isotherms were determined by batch adsorption experiments at 30°C in the dark. Briefly, various amounts of solid adsorbent were introduced into 50 mL flasks, receiving 20 mL RhB aqueous solution with an initial 50 mg/L concentration. The samples were shaken for 2 h at the same conditions in the kinetic experiment. The time was sufficient to reach apparent adsorption equilibrium based on the results of adsorption kinetics. Then the equilibrium concentration in the aqueous phase was measured. The adsorbed capacity was calculated according to equation (1):

$$Q_e = \frac{(C_i - C_e)V}{M_s} \quad (1)$$

where Q_e (mg/g) is the equilibrium adsorption capacity of adsorbent, C_i (mg/L) is the initial aqueous phase concentration, C_e (mg/L) is the equilibrium concentration, V (mL) is the volume of solution, M_s (g) is the mass of adsorbent.

A Fenton-like reaction was carried out to regenerate the saturated adsorbents. Briefly, 0.04 g adsorbents saturated by RhB were transferred into a 30 mL H_2O_2 (30 mmol/L, pH=3.0) aqueous solution and shaken for 30 min at 50°C to completely remove the adsorbed RhB molecules. The regenerated adsorbents were magnetically separated from the solution and dried for recycled adsorption tests.

Characterization

The nanometric structure and the morphology of the composites were observed by a transmission electron microscope (TEM, JEM-2100F, JEOL, Japan). The crystal structure of Fe_3O_4 and Fe_3O_4/RGO composites were measured using a powder X-ray diffraction (XRD, D/max-2200/PC, Rigaku Corporation, Japan) with Cu K_α radiation at 40 kV and 30 mA. Raman spectra were obtained on a Senterra R200-L dispersive Raman microscope (Bruker Optik Gmbh, Germany) with a 532 nm laser source. The chemical states of elements in the nanocomposites were determined by X-ray photoelectron spectroscopy (XPS, AXIS ULTRA DLD, Kratos Ltd., Japan). The Brunauer-Emmett-Teller (BET) specific surface areas of the samples were analyzed by a Micromeritics ASAP 2010 M+C nitrogen adsorption apparatus (USA). All of the samples were degassed at 180°C before nitrogen adsorption measurements were taken. Fourier transform infrared spectroscopy (FTIR) was performed at a scanning range of 4000-400 cm^{-1} on a Nicolet 6700 Infrared-Raman Spectroscope (Thermo Fisher Co., USA) with DTGS detector.

Results and discussion

Characterizations of adsorbents

The morphology and microstructure of GO and Fe_3O_4/RGO composite (M3) were characterized by TEM. As shown in Fig. 1(a), GO displays a typical flake-like and crumpled shape of graphene morphology. Corrugation and scrolling are the intrinsic nature of graphene, because its ultra-thin and large two-dimensional structure would become thermodynamically stable via bending [34-36]. The GO nanosheets are transparent and very stable under the electron beam.

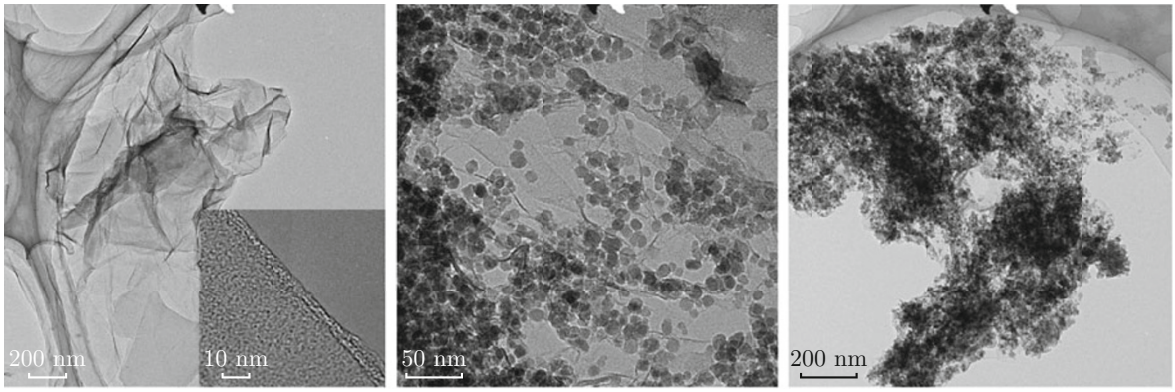

Fig. 1 (a) TEM images of GO and ((b) and (c)) Fe_3O_4/RGO composite M3. Insert in A is a HRTEM image of GO.

The ordered graphitic lattices are visible in the HRTEM image of the insert in Fig. 1(a). The folding and scrolling edges of nanosheets allow for a cross-section view of several GO layers. The TEM in Fig. 1(b) and 1(c) show that the spherical structure Fe_3O_4 nanoparticles grow over the nanosheets of RGO regularly with diameters ranging from 10 to 20 nm. The dispersion of Fe_3O_4 nanoparticles is well, and there is little observable aggregation of those nanospheres, which is attributed to the in-situ growth of Fe_3O_4 nanoparticles followed with the chemical interaction between ferric or ferrous ions and the carboxylate or hydroxyl groups.

XRD patterns were measured to study the crystal phases and components of Fe_3O_4 and the Fe_3O_4/RGO composites, as shown in Fig. 2. The presence of four characteristic peaks at about 30.1°, 35.5°, 43.1° and 57.1° are observed for all of the diffraction patterns, which are identical to the indices $d(220)$, $d(311)$, $d(400)$ and $d(511)$ of inverse spinel Fe_3O_4 (PDF No. 75-1609), respectively. No other peaks of the hematite or other crystal phase iron oxides were detected in the XRD patterns, indicating that the Fe_3O_4 nanoparticles in the as prepared composites were pure Fe_3O_4 with inverse spinel structure [37]. It can be observed that with the increases of iron oxide, the intensity of characteristic peaks in the composites is enhanced.

Figure 3 shows the Raman spectra of GO and the composite M3. In the range below 800 cm^{-1}, some bands including 215.9, 273.3, 390.7, 482.3 and 642.1 cm^{-1} appear in the spectrum of M3. These bands are also observed in the composite of Fe_3O_4/MWCNTs and attributed to the vibration modes of Fe-O and Fe-C bonds [5]. There is no observable Raman mode at around 300 or 410 cm^{-1}, indicating the absence of hematite phase in the composite [38,39]. On the other hand, Raman spectroscopy can provide information on the disorder and defect structures of carbonaceous materials. Both spectra of GO and M3 show the fundamental D and G bands of graphene at around 1340 and 1580 cm^{-1}, respectively. The former one is corresponding to A1g symmetry mode of the disordered sp^3 carbon with the structural defects, amorphous carbon, or edges that break the symmetry and selection rule, while the latter one is attributed to the in-plane vibration of sp^2-bonded carbon domains [33,40]. Moreover, the intensity ratio of the two bands (I_D/I_G) is used to measure the degree of ordering in the carbon materials.

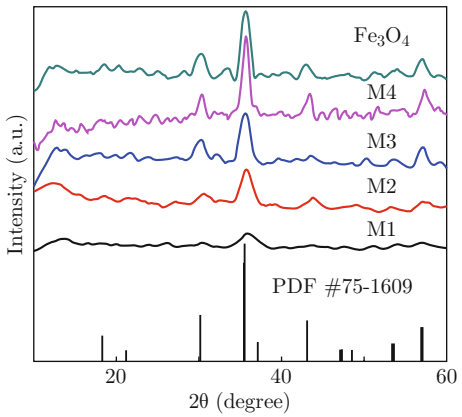

Fig. 2 XRD patterns of Fe_3O_4 and Fe_3O_4/RGO composites with various ratios (M1-M4).

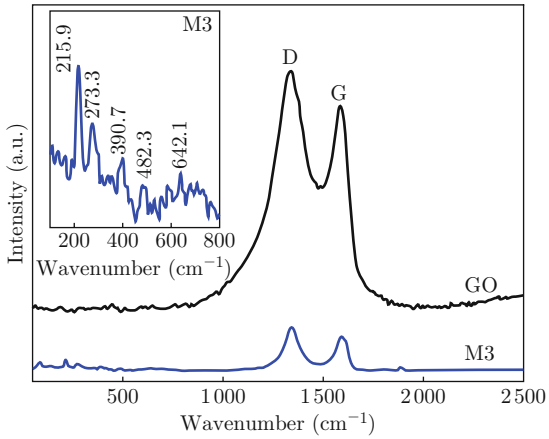

Fig. 3 Raman spectra of GO and the Fe_3O_4/RGO composite M3 (insert is the magnified region at 100-800 cm^{-1}).

The ratio I_D/I_G of GO is calculated as 2.70, indicating the presence of a large amount of sp^3 carbons in the GO nanosheets. D and G bands of GO are centered at 1332 and 1581 cm^{-1}, respectively. In comparison to GO, M3 has a much lower I_D/I_G value (1.86), and the center of the two bands red shift to 1341 and 1589 cm^{-1}, respectively. It represents that GO has been partially reduced, and there are chemical interactions, but not only physical adsorption between Fe_3O_4 nanoparticles and RGO carbon [41].

The chemical states of elements in M3 were further determined by XPS analyses, and the results are shown in Fig. 4. The binding energies of peaks at about 284, 530 and 711 eV are corresponding to the C 1s, O 1s and Fe 2p, respectively. The carbon spectrum could be deconvoluted into two bands at 284.6 and 287.3 eV, corresponding to C=C/C–C, and C=O respectively. The absence of C-O group in the nanocomposite indicates the reduction of GO. In Fig. 4(c), the two peaks at 710.9 and 724.8 eV of Fe 2p are corresponding to Fe $2p^{1/2}$ and Fe $2p^{3/2}$ of Fe_3O_4, respectively [42]. This can also be supported by the deconvoluted peak at 530.2 eV in the O 1s spectrum (Fig. 4(d)), which is the binding energy of crystal oxygen in Fe_3O_4. Another peak located at 531.8 eV can be attributed to the residual C=O group over the RGO.

N_2 adsorption-desorption isotherms for Fe_3O_4 and the composites are shown in Fig. 5. According to the IUPAC classification, Fe_3O_4 displays a type II isotherm, which is the normal form for non-porous materials. It is obviously that the composites exhibit higher N_2 adsorption quantity than pure Fe_3O_4, because the highly dispersion of Fe_3O_4 nanoparticles over the RGO support results in enhanced surface area and improved porosity and adsorb ability. The isotherm curves of the composites are quite different with Fe_3O_4 and ascribed to type IV. The sharp steps at the relative pressure around 0.4 P/P_0 is associated with capillary condensation of N_2 molecules inside the pores. However, the Type H_2 characteristic of their hysteresis loops above 0.4 P/P_0 presents that the distribution of pore size and shape is not well-defined, which appears in many typical porous adsorbents (e.g. inorganic oxide gels and porous glasses), and is attributed to the complicated mechanism related with pores with narrow necks and wide bodies and effects of the whole network [43]. M2 has the highest N_2 adsorption, corresponding to its largest specific surface area, which is found to be 296.2 m^2/g by using a BET equation, higher than 264.6 and 208.7 m^2/g for M1 and M3, respectively. Comparing to the 13.1 m^2/g surface area of Fe_3O_4 nanoparticles, the composites has significantly enhanced surface area, which

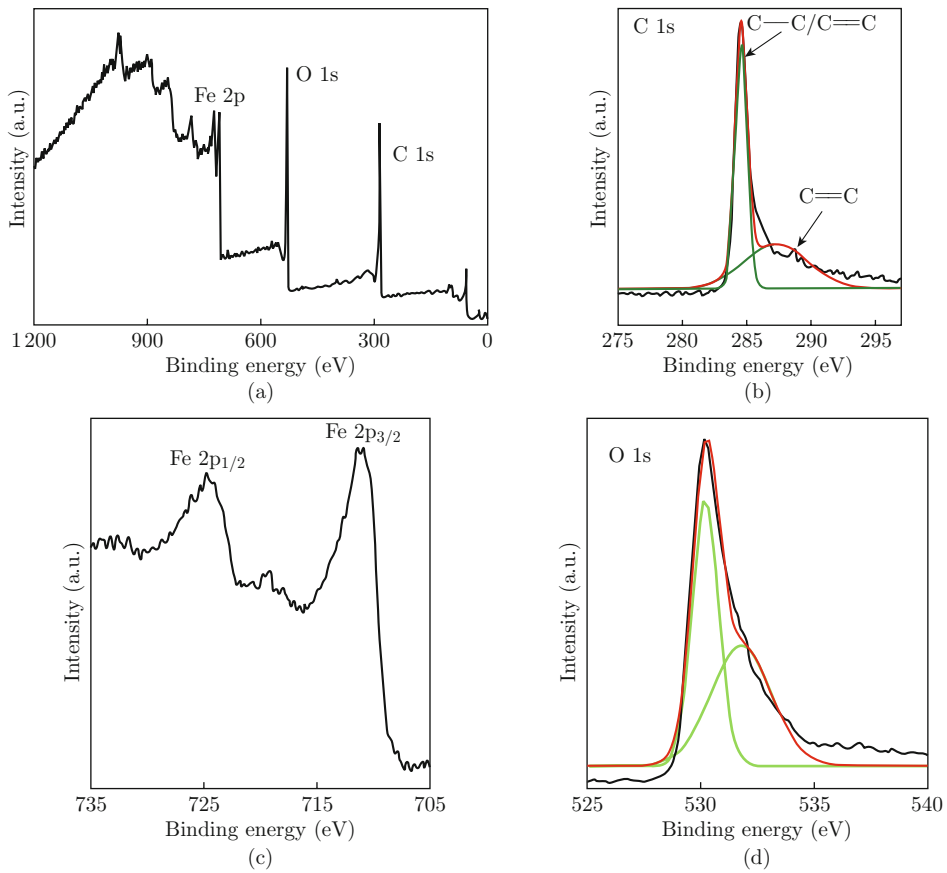

Fig. 4 (a) XPS survey spectrum of Fe_3O_4/RGO composite M3 and the corresponding high-resolution spectra of (b) C 1s; (c) Fe 2p and (d) O 1s.

is the result of the presence of two dimensional RGO nanosheets and the highly dispersive Fe_3O_4 nanoparticles over the surface of RGO. According to above analyses, the adsorbent of Fe_3O_4/RGO with tunable surface properties can be obtained by changing the dosage of iron sources.

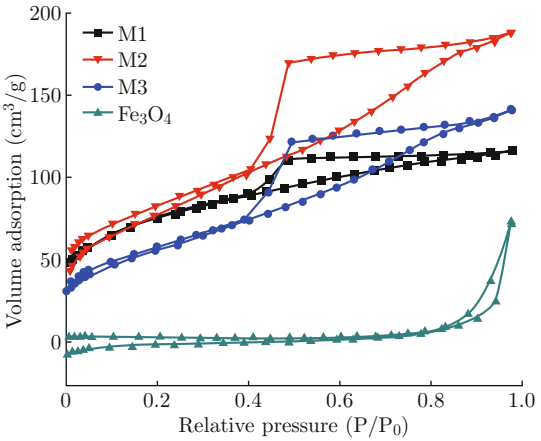

Fig. 5 Nitrogen adsorption isotherms of Fe_3O_4 and Fe_3O_4/RGO composites.

Adsorption performance of the Fe_3O_4/RGO composites

In order to evaluate the adsorption performance of the Fe_3O_4/RGO composites toward organic dyes in wastewater, the basic dye RhB was employed as the model pollutant. Figure 6 is the adsorption kinetics of RhB on various adsorbents. Fe_3O_4 nanoparticles display low adsorption capacity due to its small surface area and lack of chemical interaction between the nanoparticles and RhB molecules. The active carbon (AC) shows a high dye adsorption capacity, which can be attributed to its large surface area (>500 m^2/g), hydrophobia surface and porous structure. RhB adsorption reaches equilibrium at 300 min, achieving more than 98% RhB decolorization. As our expectation, all composites show high adsorption capacity when reaching equilibrium. However, according to Fig. 6, it is interesting to observe that the composite M1, which has the highest amount of RGO and even a larger surface area than M3, shows relatively poorer adsorption performance, both in the capacity and kinetic rate. The RhB adsorption on M1 approaches balance after more than 10 h, while the time on M2 and M3 is only 20 and 10 min, respectively. It is known that RGO has the ability to adsorb RhB efficiently at very low concentration, indicating specific interactions toward RhB molecules [24,44-46]. However, the adsorption kinetic depends much on the chemical components of RGO. Composites M2 and M3 display even better adsorption capacities and faster kinetic rates than AC, although AC has more than double surface area than the composites. It also suggests that the RhB adsorption mechanisms on AC and composites are different. Figure 6(b) shows the RhB adsorption kinetics on M3 at different pH conditions. In both acidic and basic solution, the adsorption rate and capacity show negligible decrease. The binding mechanisms of RhB on other molecular or materials have been discussed and most of them are pH dependent [46,47], including hydrogen bond, electrostatic interaction and hydrophobic interaction. Here the RhB adsorption on the composite is efficient in a wide pH range from 3.6 to 9.6. The reason is that the influences of pH on these mechanisms are different. The function of hydrogen bond is strong at acidic solution, whereas the role of electrostatic interaction would be important at basic conditions due to the more negative charged materials. In additional, in a higher pH solution, the inhibited aggregation of RhB molecules also favors a better adsorption [48]. Moreover, the planar structure of RGO and the aromatic conjugate RhB molecules renders a strong π-π stack between them, which enables the efficient adsorption work at a wide pH range.

The isotherms have been measured to explore the adsorption process. Figure 7 shows the adsorption isotherms of RhB on various adsorbents. The most frequently-used isotherm models are Langmuir and Freundlich models. The former one is represented for the

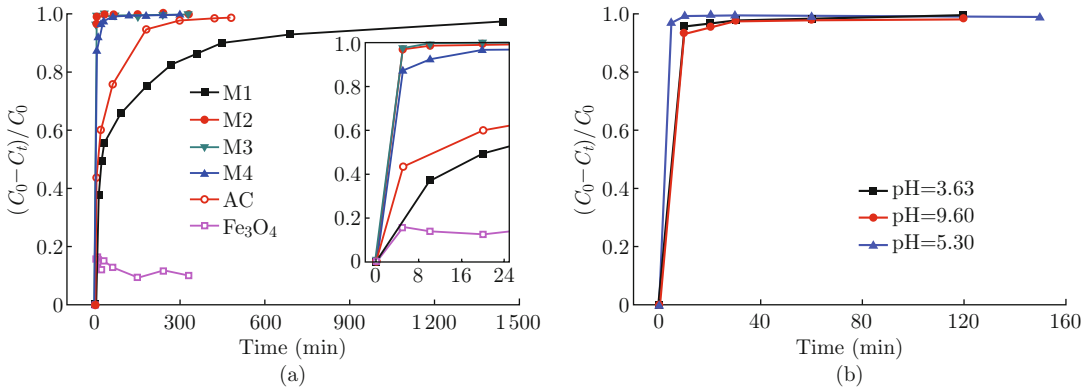

Fig. 6 (a) Adsorption kinetics for RhB on Fe_3O_4, active carbon and Fe_3O_4/RGO composites (initial concentration of RhB, 50 mg/L; adsorbent dosage, 1 g/L; pH=5.30; T=30°C); (b) RhB adsorption on M3 at different pH conditions.

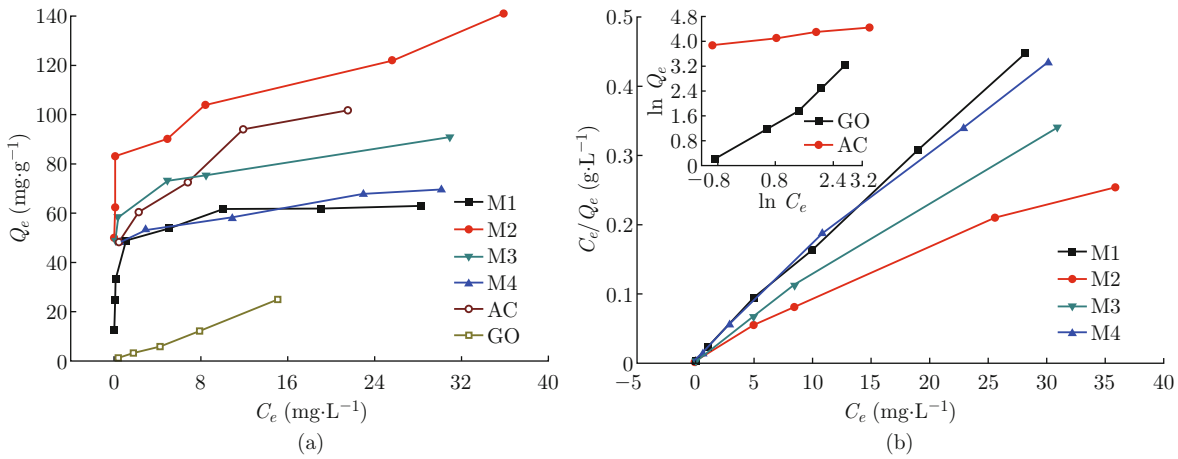

Fig. 7 Adsorption of RhB onto various adsorbents (a) and Langmuir isotherms of Fe_3O_4/RGO composites (b); inset in (b) is the Freundlich isotherms of AC and GO.

monolayer adsorption by the equation (2), whereas the latter one is described by equation (3) for the multilayer adsorption.

$$\frac{C_e}{Q_e} = \frac{1}{Q_{\max} K_L} + \frac{C_e}{Q_{\max}} \quad (2)$$

$$\ln Q_e = \ln K_f + \frac{1}{n} \ln C_e \quad (3)$$

where $Q_{\max}$ (mg/g) is the maximum adsorption capacity of adsorbent; K_L (L/mg) is the Langmuir constant related to energy of adsorption; K_f (L/g) and n are Freundlich constants corresponding to the factors affecting the adsorption capacity and intensity of adsorption, respectively. The linear fitting results and parameters by both models are listed in Table 1. According to the linear correlation coefficient in the two models, RhB adsorption on Fe_3O_4/RGO composites can be well described by Langmuir model, but poorly by Freundlich model. The fitting results suggest that RhB adsorption on composites is ascribed to monolayer adsorption, an interaction between the groups on RGO and RhB molecules playing principal role for the effective adsorption. However, the better linear fitting for active carbon and GO is Freundlich model, indicating RhB adsorptions on them are more complicated than monolayer format, which could be ascribed to the porous structure of AC and the different mechanism on RhB reduction by GO. The adsorption capacity of GO was measured by centrifuging the suspension after adsorption equilibrium. $Q_{\max}$ for GO is only 14.2 mg/g, which is comparable to the reference result [49], but much lower than those of composites. This indicates in the composites, the micro components of those carbon rings have been much altered. In the composites, M2 possesses the largest $Q_{\max}$ and smallest K_L, corresponding to its highest adsorption capacity and lowest adsorption energy. Considering the presence of Fe_3O_4 nanoparticles, we normalize the maximum adsorption capacity of adsorbent according to the carbon amount in the composites. Then $Q_{\max}$ of M2 is 432.91 mg/g, more than 3.7 times higher than AC, and at the same time the adsorption rate is about thirty times faster. However, compared to M2, M3 shows even higher adsorption rate but a little lower adsorption capacity, indicating the influent factors to adsorption rate and adsorption capacity are different. The excellent adsorption performance of composites can be attributed to the combination effects of electrostatic interactions, hydrophobic interactions and π-π stacks toward the organic conjugation molecules. However, there is only van der Waal's hydrophobic interaction for the adsorption on AC, which is relatively weak and results in a much slower adsorption rate and a smaller adsorption capacity [46,48]. It was reported that GO can act as a surfactant because of its hydrophilic edges and hydrophobic basal plane [13]. The dosage of iron source contributes to the extent of GO reduction. With the reduction, the increase of hydrophobic characteristic and yet partially retained hydrophilic groups must be one reason for the improved adsorption. A strong hydrophobic interaction toward RhB molecules induces the fast adsorption. Moreover, the enhanced π electrons in the conjugated structure of

Table 1 Fitted parameters for RhB adsorption on different adsorbents

Adsorbent	Freundlich Model			Langmuir Model			
	n	K_f/ (L/g)	R^2	$Q_{\max}$/ (mg/g)	$Q_{\max}$/ (mg/gC)	K_L/ (L/mg)	R^2
M1	6.67	41.68	0.905	66.67	133.34	3.75	0.999
M2	8.33	78.26	0.969	142.86	432.91	0.88	0.984
M3	9.09	61.91	0.966	92.08	368.32	1.28	0.995
M4	10	49.26	0.979	71.02	355.10	0.91	0.995
AC	7.69	54.67	0.989	91.66	91.66	1.74	0.974
GO	1.21	2.23	0.978	14.20	14.20	0.23	0.976

RGO lead to a facile π-π stack with the molecules with aromatic groups. Considering the fastest adsorption kinetic and relatively higher adsorption capacity of M3, this composite was chosen for the following studies.

Recycle and regeneration

The recyclable property of the composites was investigated by the magnetically separable performance and the regeneration after heterogeneous Fenton-like reaction or methanol washing. Magnetic hysteresis of M3 was measured as shown in Fig. 8. The composite has a typical ferromagnetic hysteresis, with a saturated magnetization of 51.76 emu/g. It was known that Fe_3O_4 nanoparticles can be separated at a very low magnetic field due to its superparamagnetic behavior [17]. Incorporation of Fe_3O_4 nanoparticles with RGO would makes the composites be easily separated from aqueous solution.

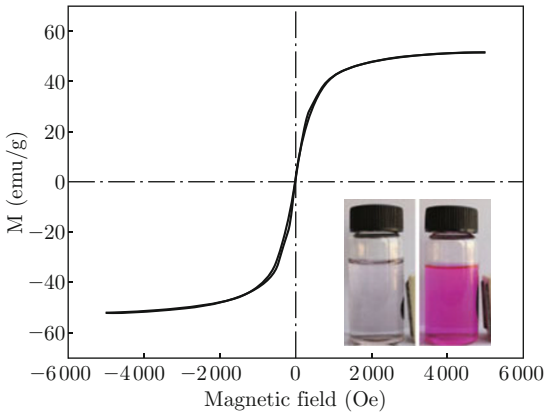

Fig. 8 Magnetic hysteresis of M3. Insert is the separation of Fe_3O_4/RGO from the solution shaken for 30 min and the initial solution under the external magnetic field.

If the adsorbent can be regenerated, the adsorbent could be repeatedly used for dyestuff wastewater purification with a low running cost. Traditional method for adsorbent regeneration is to eliminate the adsorbates by washing with a certain solution or calcining at a high temperature. However, these methods would be requiring a high cost, causing secondary pollution or time-consuming. A control test shows that the adsorbed RhB on M3 could not release into the water at a wide range of pH solution. However, the adsorbent can be regenerated by rinsing with methanol. The regenerated M3 by rinsing with methanol was used for RhB adsorption, and the adsorption performance is almost restored, as shown in Fig. 9. As we known, Fe_3O_4 in nano sizes can act as a heterogeneous Fenton-like catalyst [21,22]. According to the Haber-Weiss mechanism, the primary processes can be described by equation 4 to 6, in which the catalytic H_2O_2 decomposition includes the adsorption of H_2O_2, the reduction of Fe^{III} and the formation of radicals by Fe^{II} and Fe^{III} species [50].

$$\equiv Fe^{III} + H_2O_2 \xrightarrow{k_{ads}} \equiv Fe^{III}(H_2O_2)_{ads} \quad (4)$$

$$\equiv Fe^{III}(H_2O_2)_{ads} \xrightarrow{k_1} Fe^{II} + HO_2 + H^+ \quad (5)$$

$$\equiv Fe^{II} + H_2O_2 \xrightarrow{k_2} \equiv Fe^{III} + OH + OH^- \quad (6)$$

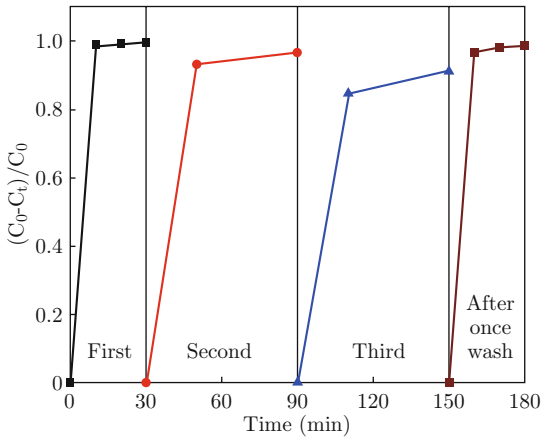

Fig. 9 The RhB adsorption on the M3 composites after Fenton-like reaction and after once wash with methanol.

Fe_3O_4/RGO composites could be a more suitable Fenton-like catalyst due to the enhanced dispersion of Fe_3O_4 nanoparticles over GO nanosheets and the concentrated RhB over the surface of adsorbents. To regenerate the adsorbent by Fenton-like reaction, the RhB saturated adsorbents were treated in H_2O_2 solution to remove adsorbed dye molecules. The final solution is colorless, indicating that adsorbed RhB was degraded and escaped from the adsorbents, which was further confirmed by the FTIR spectra, as shown in Fig. 10. Compared to the as-prepared M3, there are several obvious new bands in the spectrum of RhB saturated M3 (M3_A), such as the bands at around 821, 1331 and 1460 cm^{-1}, corresponding to the rock vibration of -CH_2-, the stretching vibration of C-N, and the bending vibration of -CH_2-, respectively [46,51]. After Fenton-like reaction, these bands originated from RhB molecules have disappeared in the sample of M3_F, indicating that RhB molecules on the adsorbent have been degraded and removed. Furthermore, the regenerated M3_F was employed for RhB adsorption to evaluate the adsorption capacity of the treated composites, as shown in Fig. 9. After twice treatments, although the RhB adsorption on M3_F becomes slower, the removal efficiency of RhB is still more than 90% after 60 min adsorption by M3_F, indicating that the adsorption capacity of M3 can be retained after regenerated by the Fenton-like treatment method. Further optimizing the conditions in the Fenton-like reaction could obtain a promising regeneration technology for Fe_3O_4/RGO adsorbents.

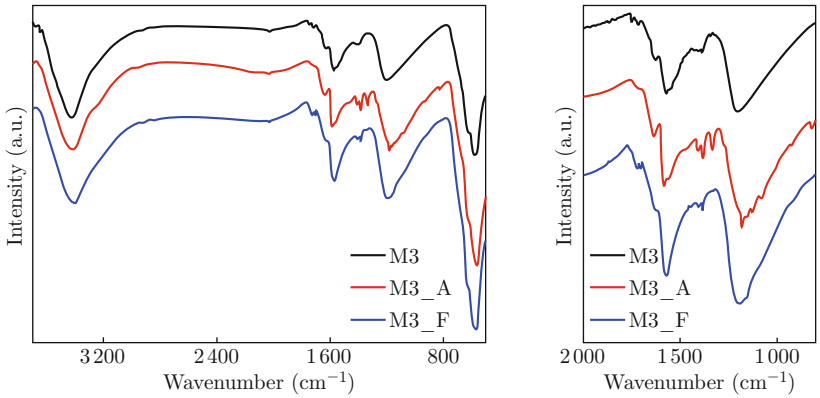

Fig. 10 (a) FTIR spectra of M3, M3 saturated by RhB (M3_A) and after Fenton reaction (M3_F); (b) Magnified region at 800-2000 cm^{-1}.

Conclusions

Effective magnetic absorbents, Fe_3O_4/RGO composites have been synthesized by an in situ coprecipitation and reduction method. Fe_3O_4 nanoparticles in sizes of 10-20 nm are well dispersed over the RGO nanosheets. According to the adsorption kinetics and isotherms toward RhB, the composite with a Fe_3O_4 to RGO ratio of 2:1 shows the highest adsorption capacity and relatively faster adsorption rate, more than 3.7 times higher and thirty times faster than commercial active carbon. Considering the monolayer RhB adsorption behavior by the Langmuir model isotherms, strong interactions between RhB molecules and RGO nanosheets, which depend much on the chemical components of RGO, contribute mainly to the surprising fast adsorption rates. Furthermore, with Fe_3O_4 nanoparticles as the heterogeneous Fenton-like catalysts, the adsorbed RhB can be degraded and removed from the adsorbents after a Fenton-like reaction, which could be developed into a promising regeneration way of adsorbents in the removal of organic molecules.

Acknowledgments

This work is financially supported by National Natural Science Foundation of China (No. 21377084) and Shanghai Municipal Natural Science Foundation (No. 13ZR1421000). We also gratefully acknowledge the support in XRD and FTIR measurements and valuable suggestions by Dr. Qunli Rao and Dr. Bangshang Zhu of the Instrumental Analysis Center of Shanghai Jiao Tong University.

References

[1] R. Sanghi and P. Verma, "Decolorisation of aqueous dye solutions by low-cost adsorbents: a review", Color. Technol. 129(2), 85-108 (2013). http://dx.doi.org/10.1111/cote.12019

[2] A. Dqbrowski, "Adsorption — from theory to practice", Adv. Colloid Interface Sci. 93(1-3), 135-224 (2001). http://dx.doi.org/10.1016/S0001-8686(00)00082-8

[3] J. C. Lazo-Cannata, A. Nieto-Márquez, A. Jacoby, A. L. Paredes-Doig, A. Romero, M. R. Sun-Kou and J. L. Valverde, "Adsorption of phenol and nitrophenols by carbon nanospheres: Effect of pH and ionic strength", Sep. Purif. Technol. 80(2), 217-224 (2011). http://dx.doi.org/10.1016/j.seppur.2011.04.029

[4] R. Liu, W. Gong, H. Lan, T. Yang, H. Liu and J. Qu, "Simultaneous removal of arsenate and fluoride by iron and aluminum binary oxide: Competitive adsorption effects", Sep. Purif. Technol. 92, 100-105 (2012). http://dx.doi.org/10.1016/j.seppur.2012.03.020

[5] X. Hu, B. Liu, Y. Deng, H. Chen, S. Luo, C. Sun, P. Yang and S. Yang, "Adsorption and heterogeneous Fenton degradation of 17α-methyltestosterone on nano Fe_3O_4/MWCNTs in aqueous solution", Appl. Catal. B: Environ. 107(3-4), 274-283 (2011). http://dx.doi.org/10.1016/j.apcatb.2011.07.025

[6] S. Tang, N. Lu, J. Li and Y. Wu, "Design and application of an up-scaled dielectric barrier discharge plasma reactor for regeneration of phenol-saturated granular activated carbon", Sep. Purif. Technol. 95, 73-79 (2012). http://dx.doi.org/10.1016/j.seppur.2012.05.002

[7] V. K. K. Upadhyayula, S. Deng, M. C. Mitchell and G. B. Smith, "Application of carbon nanotube technology for removal of contaminants in drinking water: a review", Sci. Total Environ. 408(1), 1-13 (2009). http://dx.doi.org/10.1016/j.scitotenv.2009.09.027

[8] Y. Zhu, S. Murali, W. Cai, X. Li, J. W. Suk, J. R. Potts and R. S. Ruoff, "Graphene and graphene oxide: synthesis, properties, and applications", Adv. Mater. 22(35), 3906-3924 (2010). http://dx.doi.org/10.1002/adma.201001068

[9] J. Kim, L. J. Cote and J. Huang, "Two dimensional soft material: new faces of graphene oxide", Acc.

Chem. Res. 45(8), 1356-1364 (2012). http://dx.doi.org/10.1021/ar300047s

[10] S. Wang, H. Sun, H. M. Ang and M. O. Tadé, "Adsorptive remediation of environmental pollutants using novel graphene-based nanomaterials", Chem. Eng. J. 226, 336-347 (2013). http://dx.doi.org/10.1016/j.cej.2013.04.070

[11] K. C. Kemp, H. Seema, M. Saleh, N. H. Le, K. Mahesh, V. Chandra and K. S. Kim, "Environmental applications using graphene composites: water remediation and gas adsorption", Nanoscale 5(8), 3149-71 (2013). http://dx.doi.org/10.1039/c3nr33708a

[12] Y. Zhi, G. Rungang, H. Nantao, C. Jing, C. Yingwu, Z. Liying, W. Hao, K. Eric Siu-Wai and Z. Yafei, "The prospective 2D graphene nanosheets: preparation, functionalization and applications", Nano-Micro Lett. 4(1), 1-9 (2012). http://dx.doi.org/10.3786/nml.v4i1.p1-9

[13] J. Kim, L. J. Cote, F. Kim, W. Yuan, K. R. Shull and J. Huang, "Graphene oxide sheets at interfaces", J. Am. Chem. Soc. 132(23), 8180-8186 (2010). http://dx.doi.org/10.1021/ja102777p

[14] Z. Liu, J. T. Robinson, X. Sun and H. Dai, "PEGylated nanographene oxide for delivery of water-Insoluble cancer drugs", J. Am. Chem. Soc. 130(33), 10876-10877 (2008). http://dx.doi.org/10.1021/ja803688x

[15] G. Zhao, T. Wen, C. Chen and X. Wang, "Synthesis of graphene-based nanomaterials and their application in energy-related and environmental-related areas", RSC Adv. 2(25), 9286-9303 (2012). http://dx.doi.org/10.1039/c2ra20990j

[16] L. Wan, M. Long, D. Zhou, L. Zhang and W. Cai, "Preparation and characterization of free-standing hierarchical porous TiO_2 monolith modified with graphene oxide", Nano-Micro Lett. 4(2), 90-97 (2012). http://dx.doi.org/dx.doi.org/10.3786/nml.v4i2.p90-97

[17] C. T. Yavuz, J. T. Mayo, W. W. Yu, A. Prakash, J. C. Falkner, S. Yean, L. Cong, H. J. Shipley, A. Kan, M. Tomson, D. Natelson and V. L. Colvin, "Low-field magnetic separation of monodisperse Fe_3O_4 nanocrystals", Science 314(5801), 964-967 (2006). http://dx.doi.org/10.1126/science.1131475

[18] M. Tayyebeh, A. Abbas, Z. Mohammad Ali, A. Mazaher and K. Nadia, "Application of modified silica coated magnetite nanoparticles for removal of iodine from water samples", Nano-Micro Lett. 4(1), 57-63 (2012). http://dx.doi.org/10.3786/nml.v4i1.p57-63

[19] H. Sun, L. Cao and L. Lu, "Magnetite/reduced graphene oxide nanocomposites: one step solvothermal synthesis and use as a novel platform for removal of dye pollutants", Nano Res. 4(6), 550-562 (2011). http://dx.doi.org/10.1007/s12274-011-0111-3

[20] Y. Huang and A. A. Keller, "Magnetic nanoparticle adsorbents for emerging organic contaminants", ACS Sustainable Chem. Eng. 1(1), 731-736 (2013). http://dx.doi.org/10.1021/sc400047q

[21] L. Gao, J. Zhuang, L. Nie, J. Zhang, Y. Zhang, N. Gu, T. Wang, J. Feng, D. Yang, S. Perrett and X. Yan, "Intrinsic peroxidase-like activity of ferromagnetic nanoparticles", Nat. Nanotechnol. 2(9), 577-83 (2007). http://dx.doi.org/10.1038/nnano.2007.260

[22] J. Zhang, J. Zhuang, L. Gao, Y. Zhang, N. Gu, J. Feng, D. Yang, J. Zhu and X. Yan, "Decomposing phenol by the hidden talent of ferromagnetic nanoparticles", Chemosphere 73(9), 1524-1528 (2008). http://dx.doi.org/10.1016/j.chemosphere.2008.05.050

[23] V. Chandra, J. Park, Y. Chun, J. W. Lee, I. C. Hwang and K. S. Kim, "Water-dispersible magnetite-reduced graphene oxide composites for arsenic removal", ACS Nano 4(7), 3979-3986. (2010). http://dx.doi.org/10.1021/nn1008897

[24] Z. Geng, Y. Lin, X. Yu, Q. Shen, L. Ma, Z. Li, N. Pan and X. Wang, "Highly efficient dye adsorption and removal: a functional hybrid of reduced graphene oxide-Fe_3O_4 nanoparticles as an easily regenerative adsorbent", J. Mater. Chem. 22 (8), 3527-3535 (2012). http://dx.doi.org/10.1039/c2jm15544c

[25] F. He, J. Fan, D. Ma, L. Zhang, C. Leung and H. L. Chan, "The attachment of Fe_3O_4nanoparticles to graphene oxide by covalent bonding", Carbon 48(11), 3139-3144 (2010). http://dx.doi.org/10.1016/j.carbon.2010.04.052

[26] M. Liu, C. Chen, J. Hu, X. Wu and X. Wang, "Synthesis of magnetite/graphene oxide composite and application for cobalt(II) removal", J. Phys. Chem. C. 115(51), 25234-25240 (2011). http://dx.doi.org/10.1021/jp208575m

[27] G. Xie, P. Xi, H. Liu, F. Chen, L. Huang, Y. Shi, F. Hou, Z. Zeng, C. Shao and J. Wang, "A facile chemical method to produce superparamagnetic graphene oxide-Fe_3O_4 hybrid composite and its application in the removal of dyes from aqueous solution", J. Mater. Chem. 22(3), 1033-1039 (2012). http://dx.doi.org/10.1039/c1jm13433g

[28] X. Zhou, Y. Zhang, C. Wang, X. Wu, Y. Yang, B. Zheng, H. Wu, S. Guo and J. Zhang, "Photo-Fenton reaction of graphene oxide: A new strategy to prepare graphene quantum dots for DNA cleavage", ACS Nano 6(8), 6592-6599 (2012). http://dx.doi.org/10.1021/nn301629v

[29] S. Q. Liu, B. Xiao, L. R. Feng, S. S. Zhou, Z. G. Chen, C. B. Liu, F. Chen, Z. Y. Wu, N. Xu, W. C. Oh and Z. D. Meng, "Graphene oxide enhances the Fenton-like photocatalytic activity of nickel ferrite for degradation of dyes under visible light irradiation", Carbon. 64, 197-206 (2013). http://dx.doi.org/10.1016/j.carbon.2013.07.052

[30] Y. C. Lee, S. J. Chang, M. H. Choi, T. J. Jeon, T. Ryu and Y. S. Huh, "Self-assembled graphene oxide with organo-building blocks of Fe-aminoclay for heterogeneous Fenton-like reaction at near-neutral pH: a batch experiment", Appl. Catal. B-Environ. 142, 494-503 (2013). http://dx.doi.org/10.1016/j.apcatb.2013.05.066

[31] J. J. An, L. H. Zhu, N. Wang, Z. Song, Z. Y. Yang, D. Y. Du and H. Q. Tang, "Photo-Fenton like degradation of tetrabromobisphenol A with graphene-$BiFeO_3$ composite as a catalyst", Chem. Eng. J. 219, 225-237 (2013). http://dx.doi.org/10.1016/j.cej.2013.01.013

[32] W. S. Hummers and R. E. Offeman, "Preparation of graphitic oxide", J. Am. Chem. Soc. 80(6), 1339-1339 (1958). http://dx.doi.org/10.1021/ja01539a017

[33] C. Chen, W. Cai, M. Long, B. Zhou, Y. Wu, D. Wu and Y. Feng, "Synthesis of visible light responsive graphene oxide/TiO_2 composites with p/n heterojunction ", ACS Nano 4(11), 6425-6432 (2010). http://dx.doi.org/10.1021/nn102130m

[34] G. Wang, X. Shen, B. Wang, J. Yao and J. Park, "Synthesis and characterisation of hydrophilic and organophilic graphene nanosheets.", Carbon 47(5), 1359-1364 (2009). http://dx.doi.org/10.1016/j.carbon.2009.01.027

[35] Z. J. Fan, W. Kai, J. Yan, T. Wei, L. J. Zhi, J. Feng, Y. Ren, L. P. Song and F. Wei, "Facile synthesis of graphene nanosheets via Fe reduction of exfoliated graphite oxide", ACS Nano 5(1), 191-198 (2011). http://dx.doi.org/10.1021/nn102339t

[36] P. Wang, J. Wang, T. Ming, X. Wang, H. Yu, J. Yu, Y. Wang and M. Lei, "Dye-sensitization-induced visible-light reduction of graphene oxide for the enhanced TiO_2 photocatalytic performance", ACS Appl. Mater. Interfaces 5(8), 2924-2929 (2013). http://dx.doi.org/10.1021/am4008566

[37] Y. Liu, W. Jiang, Y. Wang, X. J. Zhang, D. Song and F. S. Li, "Synthesis of Fe_3O_4/CNTs magnetic nanocomposites at the liquid–liquid interface using oleate as surfactant and reactant", J. Magn. Magn. Mater. 321(5), 408-412 (2009). http://dx.doi.org/10.1016/j.jmmm.2008.09.039

[38] X. Gou, G. Wang, J. Park, H. Liu and J. Yang, "Monodisperse hematite porous nanospheres: synthesis, characterization, and applications for gas sensors", Nanotechnol. 19(12), 125606 (2008). http://dx.doi.org/10.1088/0957-4484/19/12/125606

[39] O. N. Shebanova and P. Lazor, "Raman study of magnetite (Fe_3O_4): laser-induced thermal effects and oxidation", J. Raman Spectrosc. 34(11), 845-852 (2003). http://dx.doi.org/10.1002/jrs.1056

[40] M. Long, Y. Qin, C. Chen, X. Guo, B. Tan and W. Cai, "Origin of visible light photoactivity of RGO/TiO_2 by in situ hydrothermal growth of undergrown TiO_2 with graphene oxide", J. Phys. Chem. C. 117(32), 16734–16741 (2013). http://dx.doi.org/10.1021/jp4058109

[41] Y. He, L. Huang, J.-S. Cai, X.-M. Zheng and S.-G. Sun, "Structure and electrochemical performance of nanostructured Fe_3O_4/carbon nanotube composites as anodes for lithium ion batteries", Electrochim. Acta 55(3), 1140-1144 (2010). http://dx.doi.org/10.1016/j.electacta.2009.10.014

[42] Y. Xue, H. Chen, D. Yu, S. Wang, M. Yardeni, Q. Dai, M. Guo, Y. Liu, F. Lu, J. Qu and L. Dai, "Oxidizing metal ions with graphene oxide: the in situ formation of magnetic nanoparticles on self-reduced graphene sheets for multifunctional applications", Chem. Commun. 47(42), 11689-11691 (2011). http://dx.doi.org/10.1039/c1cc14789g

[43] K. S. W. Sing, D. H. Everett, R. A. W. Haul, L. Moscou, R. A. Pierotti, J. Rouquerol and T. Siemieniewska, "Reporting physisorption data for gas/solid systems with special reference to the determination of surface area and porosity", Pure Appl. Chem. 57(11), 2201-2218 (1982). http://dx.doi.org/10.1351/pac198254112201

[44] X. Yu, H. Cai, W. Zhang, X. Li, N. Pan, Y. Luo, X. Wang and J. G. Hou, " Tuning chemical enhancement of SERS by controlling the chemical reduction of graphene oxide nanosheets ", ACS Nano 5(2), 952-958 (2011). http://dx.doi.org/10.1021/nn102291j

[45] J. N. Tiwari, K. Mahesh, N. H. Le, K. C. Kemp, R. Timilsina, R. N. Tiwari and K. S. Kim, "Reduced graphene oxide-based hydrogels for the efficient capture of dye pollutants from aqueous solutions", Carbon 56, 173-182 (2013). http://dx.doi.org/10.1016/j.carbon.2013.01.001

[46] R. Zhang, M. Hummelgård, G. Lv and H. Olin, "Real time monitoring of the drug release of rhodamine B on graphene oxide", Carbon 49(4), 1126-1132 (2011). http://dx.doi.org/10.1016/j.carbon.2010.11.026

[47] I. Moreno-Villoslada, M. Jofré, V. Miranda, R. González, T. Sotelo, S. Hess and B. L. Rivas, "pH dependence of the interaction between rhodamine B and the water-soluble poly(sodium 4-styrenesulfonate)", J. Phys. Chem. B 110(24), 11809-11812 (2006). http://dx.doi.org/10.1021/jp061457j

[48] A. J. Ahamed, V. Balakrishnan and S. Arivoli, "Kinetic and equilibrium studies of Rhodamine B adsorption by low cost activated carbon", Arch. Appl. Sci. Res. 3(3), 154-166 (2011).

[49] G. K. Ramesha, A. V. Kumara, H. B. Muralidhara and S. Sampath, "Graphene and graphene oxide as effective adsorbents toward anionic and cationic dyes", J. Colloid Interf. Sci. 361(1), 270-7 (2011). http://dx.doi.org/10.1016/j.jcis.2011.05.050

[50] M. Xia, M. Long, Y. Yang, C. Chen, W. Cai and B. Zhou, "A highly active bimetallic oxides catalyst supported on Al-containing MCM-41 for Fenton oxidation of phenol solution", Appl. Catal. B: Environ. 110, 118-125 (2011). http://dx.doi.org/10.1016/j.apcatb.2011.08.033

[51] A. Chouket, H. Elhouichet, M. Oueslati, H. Koyama, B. Gelloz and N. Koshida, "Energy transfer in porous-silicon/laser-dye composite evidenced by polarization memory of photoluminescence", Appl. Phys. Lett. 91(21), 211902 (2007). http://dx.doi.org/10.1063/1.2814051